ISSN 0915-633X

NATIONAL INSTITUTE FOR FUSION SCIENCE

Kinetic Approach to Long Wave Length Modes in Rotating Plasmas

T. Yamagishi

(Received – Feb. 20, 1992)

NIFS-138

Mar. 1992

RESEARCH REPORT
NIFS Series

NAGOYA, JAPAN

Kinetic Approach to Long Wave Length Modes in Rotating Plasmas

T.Yamagishi
Fukui Institute of Techology
Gakuen Fukui 910

Abstract

Stability of low frequency long wave length modes is studies by a kinetic approach in rotating Maxwellian plasmas. In the rigid rotator model, the centrifugal force due to the plasma rotation strongly destabilizes the ballooning modes particularly when the Mach number is close to unity. The fluid flow shear weakly stabilizes the ballooning mode. Energetic particles are effective to stabilize the ballooning mode particurarly in the high-β region even in the rotating plasmas. The electric potential induced from the radial electric field increases the particle trapping rate for $e\Phi>0$. For $\Phi<0$ as in tokamaks, electron trapping rate increases, which destabilizes the dissipative trapped electron mode.

Keywords: Radial electric field, plasma rotation, electric potential, drift kinetic solution, electromagnetic perturbations, Krook collision term, ballooning mode, drift resistive ballooning mode, passing particles, trapped particles, energetic particles, centrifugal force, fluid flow shear, disspative trapped electron mode.

§1. Introduction

Recently plasma state in the presence of radial electric field in tokamaks is paid attention in connection with the H-mode experiments[1)2)]. The radial electric field is also produced in helical hystems[3)]. It may be induced by the unbalance of electron and ion transports, and also by the momentum balance in the neutral beam injections. The plasma state in the steady electric field is interesting and important, because the steady electric field modifies particles orbits and also affects plasma neutrality significantly.

When the radial electric field E_r exists, plasma particles suffer ExB drift motion. In the toroidal system, the ExB drift motion makes plsama rotation in the poloidal and toroidal directions, since the drifts are the same direction both for electron and ion. In the laboratory system, this plasma rotation makes the Doppler frequency shift. On the other hand, the plasma rotation makes the centrifugal force in the radial direction, and therefore, the ion drift motion. Since the ballooning mode is induced by the precessional drift motion due to the centrifugal force of particles moving along the magnetic field lines, and since the plasma rotation also makes the centrifugal force, the ballooning mode may be modified in the rotating plasmas which may becomes important when the rotation speed $v_E=-cE_r/B$ becomes comparable to ion thermal speed, which has been experimentally observed in tokamaks. Both the centrifugal forces of particle moving along the magnetic field lines and plasma rotation are outward direction, the plasma rotation may destabilize the ballooning mode. The ballooning mode stability in the rotating plasmas has been studied by many authors[4)~8)]. In this report, we study long wave length modes by kinetic approach assuming the Maxwellian plasmas.

When the the electric field E_r exists, through the relation $E_r=-d\Phi/dr$, the elctric potential Φ also exists, which modifies plasma

particle dynamicis. For $\Phi<0$ as in tokamaks[9], more electrons and less ions may be trapped by the electromagnetic potential which may modifies the neutrality condition. Trapped electron mode may be destabilizes by the electric potential. We will also consider this problem in §4.

§2. Perturbed Distribution Function

We first derive the distribution function f_1 which is the solution of the first order perturbation of the Vlasov equation in the usual toroidal coordinate system (r,θ,φ). In terms of the perturbed electric field $\mathbf{E}_1$ and magnetic field $\mathbf{B}_1$, the purturbed distribution function f_1 may be given by the particle orbit intergral form:

$$f_1 = -\frac{e}{M}\int_{-\infty}^{t} dt' (\mathbf{E}_1 + \frac{1}{c}\mathbf{v}\times\mathbf{B}_1)\frac{\partial f_0}{\partial \mathbf{v}} \tag{1}$$

The unperturbed distribution function f_o for the rotating plasma in the poloidal direction is assumed to be given in the form[10]

$$f_0 = (\pi v_{th}^2)^{-\frac{3}{2}} \exp(-\frac{v^2 - 2Gx}{v_{th}^2})(1 - \frac{\gamma}{L'}) \tag{2}$$

where v_{th} is the thermal velocity which is related to temperature T by $T=Mv_{th}^2/2$ with M being particle mass, G is the gravity of particle in the radial direction, x is the radial coordinate from the rational suface $r=r_o$, i.e., $x=r-r_o$, $\gamma = x+v_\theta/\Omega$, and all other notations are standard.

The quantities $\alpha=v_\perp^2-2Gx$ and γ are the invariant of particle motion just like the total energy $E=Mv^2/2+e\Phi$ and angular momentum $\mu=Mv_\perp^2/2B$, i.e., they are constant of particle motion , $d\alpha/dt=0$, etc. In eq.(2), L' is the scale length of density variation L and the

curvature of the gravity at x=0:

$$\frac{1}{L}=\frac{1}{N}\frac{d}{dr}\left(\int d^3v f_0\right)=\frac{1}{L'}+\frac{2G}{V_{th}^2} \tag{3}$$

We assume that the radial component of gravity G consists of the radial electric field E_r, and the centrifugal forces of particle motion along magnetic field (source of ballooning mode) and the plasma rotation in the poloidal direction due to the ExB drift motion:

$$G=\frac{e}{M}E_r+\frac{V_{th}^2}{R}+\frac{V_E^2}{r} \tag{4}$$

where $\mathbf{v}_E=c(\mathbf{E}_1\times\mathbf{B})/B^2$.

For the low-beta ($\beta<<1$) plasmas, we assume that the pertubed vector potential consists of only parallel component: $\mathbf{A}_1=A_\parallel\mathbf{b}$ with $\mathbf{b}=\mathbf{B}/B$, and the radial component of perturbed magnetic field is given by $\mathbf{B}_1=ik_\theta A_\parallel\mathbf{e}_r$. In this case, the perturbed electric field becomes $\mathbf{E}_1=-\nabla\phi+i\omega A_\parallel\mathbf{e}_\phi/c$ with ϕ being perturbed scalar potential. From eq.(2), at x=0, we have

$$\frac{\partial f_0}{\partial \mathbf{v}}=-\left(\frac{2}{v_{th}^2}\mathbf{v}+\frac{1}{\Omega L'}\mathbf{e}_\theta\right)f_0 \tag{5}$$

Applying eq.(5) to eq.(1), we have the perturbed distribution in the form

$$f_1=-\frac{e}{T}\phi-i\frac{e}{T}\int_{-\infty}^{t}dt'\left(\omega-\frac{k_\theta T}{M\Omega L'}\right)\left(\phi-\frac{V_\parallel}{c}A_\parallel\right)f_0 \tag{6}$$

Making use of eqs.(3) and (4), the frequency $k_\theta T/M\Omega L'$ in eq.(6) can be decomposed into four portions:

$$\frac{k_\theta T}{M\Omega L'}=\omega_E+\omega_D+\omega_g+\omega^* \tag{7}$$

where $\omega_E=k_\theta v_E$ with $v_E=cE_r/B$ is the plasma rotation frequency due to ExB drift motion, $\omega_d=-k_\theta v^2/2\Omega R$ is the curvature drift frequency, $\omega_g=-k_\theta v_E^2/2r\Omega$ is the drift frequency due to the rotational centrifugal force, and $\omega^*=k_\theta cT/eBL$ is the diamagnetic drift frequency.

Expanding the perturbed scalar potential ϕ and vector potential $A_{\parallel}$ in Fourier series, taking into account the particle orbit information in the toroidal system to the eikonal by the same method as in Ref.(11) for low frequency regime $\omega<<\Omega=eB/Mc$, from eq.(6), we obtain the Fourier coefficient of the perturbed distribution f_1 in the form

$$\hat{f}=-\frac{e}{T}f_0\left[\hat{\phi}-J_0^2(a)\frac{\omega-\omega_E-\omega_D-\omega_g-\omega^*}{\omega-\omega_E-\omega_D-\omega_g-k_\parallel v_\parallel}\left(\hat{\phi}-\frac{v_\parallel}{c}A_\parallel\right)\right] \tag{8}$$

where J_0 is the Bessel function and $a=k_\perp v_\perp/\Omega$. The terms $-\omega_E-\omega_D-\omega_g$ in the numerator in eq.(8) is induced from the gravity in eq.(4). In usual theory without the electric field, these terms are absent.

§3. Effect of Plasma Rotation on Ballooning Modes

We now proceed to derivation of electromagnetic dispersion relation for rotating plsamas making use of the distribution function given by eq.(8). For the sake of simplicity, we assume $T_e=T_i=T$. In this case, from the definitions, $\omega^*_e=-\omega^*_i=\omega^*>0$, $\omega_{De}=-\omega_{Di}=\omega_D>0$ and $\omega_{ge}<<\omega_{gi}=\omega_g<0$. While ω_E is the same for both ion and electron. The frequency ω in eq.(8) is shifted by ω_E. We express the Doppler shifted frequency by $\bar{\omega}=\omega-\omega_E$. From eq.(8), the perturbed distribution function for ion can be written in terms of electron's characteristic frequencies as follows

$$\hat{f}_i=-\frac{ef_0}{T}\left[\hat{\phi}-J_0^2(a)\frac{\bar{\omega}+\omega_D-\omega_g+\omega^*}{\bar{\omega}+\omega_D-\omega_g-k_\parallel v_\parallel}\left(\hat{\phi}-\frac{v_\parallel}{c}A_\parallel\right)\right] \tag{9}$$

For electrons, taking into account the Krook type collision, neglecting the finite Larmor radius effect, $J_0 \to 1$, and the centrifugal force effect, from eq.(8), we have

$$\hat{f}_e = \frac{e}{T} f \left[\hat{\phi} - \frac{\bar{\omega} - \omega_D - \omega^*}{\bar{\omega} - \omega_D - k_\parallel v_\parallel + i\nu_e} \left(\hat{\phi} - \frac{v_\parallel}{c} \hat{A}_\parallel \right) \right] \tag{10}$$

where ν_e is the collision frequency.

Integrating eq.(9) over the velocity space, neglecting trapped particles, we have the perturbed ion density:

$$n_i = -\frac{eN}{T} \left[\hat{\phi} + \frac{\bar{\omega} + \omega_D - \omega_g + \omega^*}{k_\parallel v_i} \Gamma_0(b) \left\{ Z_0(\zeta_i) \hat{\phi} - Z_1(\zeta_i) \frac{v_i}{c} \hat{A}_\parallel \right\} \right] \tag{11}$$

where v_i is the ion thermal velocity, $\Gamma_0(b) = I_0(b) \exp(-b)$ with I_0 being the modified Bessel function, $b = k_\perp^2 \rho_i^2 / 2$,

$$Z_p(\zeta) = \frac{1}{\sqrt{\pi}} \int_{-\infty}^{\infty} dy \frac{y^p}{y - \zeta} e^{-y^2} \tag{12}$$

is the p-th moment of the plsma dispersion function, and $\zeta_i = (\omega + \omega_D - \omega_g) / k_\parallel v_i$. By the same manner, we have the perturbed electron density:

$$n_e = \frac{eN}{T} \left[\hat{\phi} + \frac{\bar{\omega} - \omega_D - \omega^*}{k_\parallel v_e} \left\{ Z_0(\zeta_e) \hat{\phi} - Z_1(\zeta_e) \frac{v_e}{c} \hat{A}_\parallel \right\} \right] \tag{13}$$

where v_e is the electron thermal velocity and $\zeta_e = (\omega + \omega_D + i\nu_e) / k_\parallel v_e$.

The quasi-neutrality condition, $n_i = n_e$, from eqs.(11) and (12), yields a relation between ϕ and $A_\parallel$:

$$\hat{\phi} = \frac{1}{D_{es}} \left| (\bar{\omega} + \omega_D - \omega_g + \omega^*) \Gamma_0(b) Z_1(\zeta_i) + (\bar{\omega} - \omega_D - \omega^*) Z_1(\zeta_e) \right| \frac{\hat{A}_\parallel}{c k_\parallel} \tag{14}$$

where D_{es} is the electrostatic part of the dispersion function:

$$D_{es}=2+\frac{\bar{\omega}+\omega_D-\omega_g+\omega^*}{k_\parallel v_i}\Gamma_0(b)\,Z_0(\zeta_i)+\frac{\bar{\omega}-\omega_D-\omega^*}{k_\parallel v_e}Z_0(\zeta_e) \tag{15}$$

Introducing eqs.(9) and (10) into the parallel compornent of Ampere's law:

$$\nabla^2\hat{A}_\parallel=-\frac{4\pi}{c}e\int v_\parallel(\hat{f}_i-\hat{f}_e)\,d^3v \tag{16}$$

we obtain another relation between ϕ and $A_\parallel$:

$$k_\parallel^2\hat{A}_\parallel=\frac{k_D^2}{ck_\parallel}\left[\left\{(\bar{\omega}+\omega_D-\omega_g+\omega^*)(\bar{\omega}+\omega_D-\omega_g)Z_1(\zeta_i)\Gamma_0(b)+(\bar{\omega}-\omega_D-\omega^*)(\bar{\omega}-\omega_D+i\nu_e)Z_1(\zeta_e)\right\}\frac{\hat{A}_\parallel}{ck_\parallel}\right]$$
$$-\left[\left\{(\bar{\omega}+\omega_D-\omega_g+\omega^*)Z_1(\zeta_i)\Gamma_0(b)+(\bar{\omega}-\omega_D-\omega^*)Z_1(\zeta_e)\right\}\hat{\phi}\right] \tag{17}$$

where $k_D^2=4\pi Ne^2/T$ is the square of the Debye wave number. Substitution of eq.(14) into eq.(17) yields an eigenmode equation

$$k_\parallel\left|\frac{ck_\parallel}{k_D}\right|^2k_\parallel\psi+\left[\frac{1}{D_{es}}\left\{(\bar{\omega}+\omega_D-\omega_g+\omega^*)Z_1(\zeta_i)\Gamma_0(b)+(\bar{\omega}-\omega_D-\omega^*)Z_1(\zeta_e)\right\}^2\right.$$
$$-\left\{(\bar{\omega}+\omega_D-\omega_g+\omega^*)(\bar{\omega}+\omega_D-\omega_g)Z_1(\zeta_i)\Gamma_0(b)+(\bar{\omega}-\omega_D-\omega^*)\times\right\}$$
$$\left.\times(\bar{\omega}-\omega_D+i\nu_e)Z_1(\zeta_e)\right\}\Big|\psi=0 \tag{18}$$

where $\psi=(ck_\parallel)^{-1}A_\parallel$. Without magnetic perturbation $\psi=0$, the dispersion relation is reduced to the electrostatic one: $D_{es}=0$.

In the incompressible regime, $\zeta_e\ll\zeta_i\ll1$, the dispersion functions Z_0 and Z_1 are approximated by $Z_0(\zeta_i)=i\pi^{1/2}$ and $Z_1(\zeta_i)=1+\zeta_iZ_0(\zeta_i)=1$. In this case, from eq.(15), $D_{es}=2$, and applying $ik_\parallel=\nabla_\parallel$, from

eq.(18), we have the ballooning mode equation for b<<1:

$$\nabla_{\perp}\left|\frac{ck_{\perp}}{k_D}\right|^2\nabla_{\perp}\psi+\left\{b\bar{\omega}^2+(iv_e+b\omega^*-b\omega_g)\bar{\omega}+2(\omega_D-\frac{1}{2}\omega_g)(\omega^*+\omega_D-\frac{1}{2}\omega_g)\right.$$
$$\left.-iv_e(\omega^*+\omega_D)+b\omega_D(\omega_g-\omega^*-\omega_D)\right\}\psi=0 \qquad (19)$$

The expression in the curly braces in eq.(19) has been confirmed by using Mathematica[12]. Neglecting the plasma rotation and collision in eq.(14), we have the usual ballooning mode equation:

$$\nabla_{\perp}\left|\frac{ck_{\perp}}{k_D}\right|^2\nabla_{\perp}\psi+\left\{b\omega(\omega+\omega^*)+2\omega^*\omega_D\right\}\psi=0 \qquad (20)$$

The first term in eq.(19) is the field line bending term which always stabilizes the MHD modes. The first term in the curly braces in eq.(20) is the inertial term, while the second term is the source of ballooning mode instabilities. Averaging eq.(19) over the extended poloidal angle θ, we have a dispersion relation

$$\bar{\omega}^2+(i\frac{v_e}{b}+\omega^*-\omega_g)\bar{\omega}+\frac{2}{b}(\omega_D-\frac{1}{2}\omega_g)(\omega^*+\omega_D-\frac{1}{2}\omega_g)-i\frac{v_e}{b}(\omega^*+\omega_D) \qquad (21)$$
$$+\omega_g\omega_D-\omega_D\omega^*-\omega_D^2-\omega_A^2=0$$

which has been confirmed by using Mathematica. In eq.(21), $\omega_A^2 = \langle k_{\parallel}^2\rangle v_A^2$ is the square of the Alfven frequency which is always stabilizing the ballooning mode, $b=\rho_i^2\langle k_{\perp}^2\rangle/2$, and the angular brackets represent the average defined by

$$\langle f\rangle=\frac{1}{2\pi}\oint f\psi^2 d\theta$$

The collision effect in the second term in eq.(21) represents the effect of collision damping, i.e., it always stabilizes the ballooning mode. While the collision effect in $-iv_e\omega_D$ is the source of drift resistive ballooning mode, which is destabilizing in the high-β regime. Since $\omega_g<0$, the plasma rotation always increases the source

of ballooning mode ω_D in the third term in eq.(21). The plasma rotation destabilizes the ballooning mode.

The dispersion relation (21) involves the drift ballooning, resistive ballooning and drift resistive ballooning modes. We consider each case separately.

(1) **Ideal Ballooning Mode.** If we neglect ν_e, ω_g and ω^{*2} in eq.(21), we have $\bar{\omega}=0$ or $\omega=\omega_E$ and the growth rate

$$\gamma=\left(\frac{2\omega^*\omega_D}{b}-\omega_A^2\right)^{\frac{1}{2}} \tag{22}$$

which clearly indicates that the first term is the source of ballooning mode, and the field line bending energy ω_A^2 is stabilizing. If we keep ω_g, eq.(21) yields $\omega=\omega_E+\omega_g/2$ and the growth rate

$$\gamma=\left(\frac{2}{b}\left(\omega^*+\omega_D-\frac{1}{2}\omega_g\right)\left(\omega_D-\frac{1}{2}\omega_g\right)-\omega_A^2\right)^{\frac{1}{2}} \tag{23}$$

Since $\omega_g<0$, ω_g increases the source of ballooning mode $\omega^*\omega_D$, i.e., the centirifugal force due to plasma rotation destabilizes the ballooning mode.

Variation of the growth rate normalized by ω^* as a function of β and the shear parameter s is presented in Fig.1 for the ideal MHD case. In numerically calculating eq.(22), the parameter b for the finite Lamor radius effect has been expressed in term of β: $b=\beta/2(c/\omega_{pi})^2\langle k_\perp^2\rangle$. The normalized Alfven frequency is also expressed in term of β: $(\omega_A/\omega^*)^2=4L_n/\beta^2(\omega_{pi}/ck_\theta)^2\langle k_\parallel^2\rangle$ with ω_{pi} being the ion plsama frequecy and $L_n=|d\ln N/dr|^{-1}$. The following averaged formulae[1] for a simple strong ballooning mode trial function: $\psi=(2/3)^{1/2}(1+\cos\theta)$ for $|\theta|<\pi$, otherwise $\psi=0$, have also been applied

$$\langle k_\perp^2 \rangle = k_\theta^2 \left(1 + (\frac{\pi^2}{3} - 2.5)\, s^2 - \frac{10}{9}\alpha s + \frac{5\alpha^2}{12} \right)$$

$$\langle k_r^2 \rangle = \frac{1 + s^2(\pi^2/3 - 0.5) - 8\alpha s/3 + 3\alpha^2/4}{3(qR)^2 (1 + s^2(\pi^2/3 - 2.5) - 10s\alpha/9 + 5\alpha^2/12)}$$

$$\langle \omega_D \rangle = \omega^* e_n \left(\frac{2}{3} + \frac{5s}{9} - \frac{5\alpha}{12} \right)$$

where $\alpha = -q^2 R d\beta/dr = q^2 R\beta/e_n$, $s = d\ln q/d\ln r$, $e_n = (Rd\ln N_0/dr)^{-1}$, and $k_\theta = m/r$ with m being the poloidal mode number. The growth rate normalized by ω^* versus β is plotted in Fig.2 for different values of the plasma rotation effect ω_g/ω^*, in which $\omega_g = 0$ means the ideal MHD without rotation. As seen in Fig.2, the centrifugal force effect due to plasma rotation increases not only the growth rate but also the unstable β-region. In these numerical calculations, $(ck_\theta/\omega_{pi})^2 = 1$ has been assumed. Since $(ck_\theta/\omega_{pi})^2 = (ck_\theta/\omega_{pe})^2 M_i/M_e$ and the plasma skin depth $c/\omega_{pe} = 0.05$ cm for $N = 10^{14}$ cm^{-3}, $(ck_\theta/\omega_{pi})^2 = 1$ means high poloidal mode number $m = 22$ for the plsama radius $a = 50$ cm.

(2) **Drift Ballooning Mode**. In this case, we neglect ω_g , ν_e in eq.(21), which yields $\omega = \omega_E - \omega^*/2$ and the growth rate

$$\gamma = \left(\frac{2\omega^* \omega_D}{b} - \omega_A^2 - \frac{1}{4}\omega^{*2} \right)^{\frac{1}{2}} \tag{24}$$

in which $\omega^{*2}/4$ is weakly stabilizing.

(3) **Resistive Ballooning Mode**. In this case, we neglect ω_g, ω^{*2} in eq.(21), which yields $\omega = \omega_E$ and the growth rate

$$\gamma = -\frac{\nu_e}{2b} + \left(\frac{2\omega^* \omega_D}{b} + \left(\frac{\nu_e}{2b} \right)^2 - \omega_A^2 - i\frac{\omega_D \nu_e}{b} \right)^{\frac{1}{2}} \tag{25}$$

The term $(\nu_e/2b)^2$ in the square root in eq.(25) is destabilizing, but

$-\nu_e/2b$ in the first term is stabilizing. In total, they are stabilizing or collision damping. The last term in the square root is destabilizing, i.e., $\omega_D\nu_e$ is the source of resistive ballooning mode. Without the collision damping ($\nu_e/2b\rightarrow 0$) at the ideal mode marginal state: $\omega_A{}^2=2\omega^*\omega_D/b$, eq.(25) yields $\omega=(\omega_D\nu_e/2b)^{1/2}$ and $\gamma=(\omega_D\nu_e/2b)^{1/2}$, i.e., $\omega=\gamma$.

(4) **Drift Resistive Ballooning Mode**. Keeping all terms in eq.(21), we have $\omega=\omega_E-(\omega^*-\omega_g)/2$ and the growth rate

$$\gamma=-\frac{\nu_e}{2b}+\left\{\frac{2}{b}\left(\omega^*+\omega_D-\frac{1}{2}\omega_g\right)\left(\omega_D-\frac{1}{2}\omega_g\right)+i\frac{\nu_e}{b}\left(\omega^*-\omega_D\right)-\omega_A^2-\frac{1}{4}\left(\frac{\nu_e}{b}+\omega^*\right)^2\right\}^{\frac{1}{2}} \qquad (26)$$

The normalized growth rate as a function of β is plotted in Fig.3 for different vales of collision frequency ν_e. As seen in Fig.3, the collision ν_e reduces the growth rate, the second stability boundary is increased, i.e., the collsion destabilizes the ballooning mode slightly in the high-β region. Variation of the normalized growth rate as a function of β and s is presented by surface graphics in Fig.4.

§4. Effect of Electric Potential

4.1 Particle Trapping Rate

When the electric potential Φ exists, the total particle energy is given by the sum of kinetic and potential energies: $E=mv_\perp{}^2/2+\mu B+e\Phi$. The parallel velocity along the magnetic field lines can be written by

$$v_\parallel=\pm\left\{\frac{2}{M}\left(E-\mu B-e\Phi\right)\right\}^{\frac{1}{2}} \qquad (27)$$

where $\mu=Mv_\perp{}^2/2B$ is the angular momentum which is an invariant of

motion like total energy E.

For tokamak magnetic field $B=B_0(1-\varepsilon\cos\theta)$ with $\varepsilon=r/R$ being the inverse aspect ratio, the parallel velocity $v_{\parallel}$ versus the poloidal angle θ is schematically shown in Fig.5. If we neglect the drift motion which may become important in high energy region, the boundary between particle trapping and passing regions may be given by $\cos\theta=-1$ and $v_{\parallel}=0$, which yields the condition

$$v_{\parallel}=\left(\varepsilon v_{\perp}^2+\frac{2e\Phi}{M}\right)^{\frac{1}{2}} \tag{28}$$

Without the electric potential, $\Phi\to 0$, eq.(27) reduces to the usual result $v_{\parallel}=\varepsilon^{\frac{1}{2}}v_{\perp}$. For $v_{\parallel} < \varepsilon^{1/2}v_{\perp}$, particles are magnetically trapped. While for $v_{\parallel} > \varepsilon^{1/2}v_{\perp}$, they are circulating.

When $\Phi\neq 0$, by the same manner, particles are trapped by the electromagnetic potential for $v_{\parallel} < (ev_{\perp}^2+2e\Phi/m)^{1/2}$, while for $v_{\parallel} > (ev_{\perp}^2+2e\Phi/m)^{1/2}$ they are circulating. The boundaries given by eq.(28) for $e\Phi<0$, $e\Phi>0$, and $e\Phi=0$ in the velocity space are shown in Fig.6. As seen in Fig.6, the "loss cone" becomes smaller for $e\Phi>0$, i.e., more particles are trapped. While for $e\Phi<0$ less particles are trapped.

Taking into account the boundary condition (28), the trapping rate of particles $P_t=\int d^3v f_0/N$ for $e\Phi>0$ is givn by

$$P_t(\varepsilon,\Phi)=\mathrm{erf}\left(\sqrt{\frac{e\Phi}{T}}\right)+\sqrt{\varepsilon_T}\left(1-\mathrm{erf}\left(\sqrt{\frac{e\Phi}{T\varepsilon}}\right)\right)\exp\left(\frac{e\Phi}{\varepsilon T}\right) \tag{29}$$

where erf(z) is the error function and $\varepsilon_T=\varepsilon/(1+\varepsilon)$. In the limit $\Phi\to 0$, eq.(29) reduces to the usual result $P_t=\varepsilon_T^{1/2}$. In the opposite limit $\varepsilon\to 0$, the second term in eq.(29) tends to zero, because from the Lopital theorem:

$$\lim_{\varepsilon\to 0}\left(1-\mathrm{erf}\left(\sqrt{\frac{e\Phi}{T\varepsilon}}\right)\right)\exp\left(\frac{e\Phi}{\varepsilon T}\right)=-\frac{2}{\sqrt{\pi}}$$

Even without the magnetic mirror effect $\varepsilon \to 0$, particle can be trapped purely by the electric potential:

$$P_t = \mathrm{erf}\left(\sqrt{\frac{e\Phi}{T}}\right) \qquad \text{for } \varepsilon \to 0. \tag{30}$$

Variation of P_t as a function of ε and $e\Phi/T$ is shown by surface graphics in Fig.7, in which one will see how much particles are trapped by the combination of the toroidal effect ε and electric potential Φ.

For $e\Phi<0$, the trapping rate is reduced, and simply given by

$$P_t = \sqrt{\varepsilon_T}\exp\left(\frac{e\Phi}{\varepsilon T}\right) \tag{31}$$

which also reduces to the usual result $P_t=\varepsilon_T^{1/2}$ for $\Phi \to 0$. In the limit $\varepsilon \to 0$, $P_t \to 0$ because $e\Phi<0$.

In tokamaks, we assume a negative eletric potential $\Phi<0$ as observed in ISX[9]. In this case, $e\Phi>0$ corresponds to electron, while $e\Phi<0$ corresponds to ion, i.e., when $\Phi<0$, more(less) electrons(ions) may be trapped by the presence of electric potential.

4.2 Dissipative Trapped Electron Mode

Let us here consider the effect of electric potential on the dissipative trapped electron mode which is essentially electrostatic. For the drift mode regime, $k_\parallel v_i \ll \omega \ll k_\parallel v_e$, neglecting passing electrons the perturbed electron density may, from eq.(13), be written as

$$n_e = \frac{e\phi}{T} N\left(1 - \frac{\omega-\omega^*}{\omega+iv_{eff}} P_t\right) \tag{32}$$

From eq.(11), the perturbed ion density becomes

$$n_i = -\frac{e\phi}{T} N \left\{ 1 - \left(1 + \frac{\omega^*}{\omega}\right) \Gamma_o(b) \right\} \tag{33}$$

The quasi-neutrality condition, $n_e = n_i$, yields the dispersion relation for $\omega > \nu_{eff}$:

$$2 - \left(1 + \frac{\omega^*}{\omega}\right) \Gamma_o(b) - \left(1 - \frac{\omega^*}{\omega}\right)\left(1 - i\frac{\nu_{eff}}{\omega}\right) P_t = 0 \tag{34}$$

Introducing $\omega = \omega_r + i\gamma$ into eq.(34), and solving for the frequency ω_r and growth rate γ with $\omega_r >> \gamma$, we have

$$\omega_r = \frac{\omega^* (\Gamma_o - P_t)}{2 - \Gamma_o(b) - P_t} \tag{35}$$

$$\gamma = \frac{2\nu_{eff}(1 - \Gamma_o) P_t}{(2 - \Gamma_o - P_t)(\Gamma_o - P_t)} \tag{36}$$

Since the electron trapping rate P_t is increasing function with respect to $e\Phi/T$ as seen in Fig 7, the electric potential destabilizes the dissipative trapped electron mode, which can also be seen in Fig.8. The singularity of γ as in the case of b=0.5 in Fig.8 occurs when $\Gamma_O = P_t$.

4.3 Ballooning Mode

We now consider the effect of electric potential on trapped electrons and apply for the stability of electromagnetic ballooning mode. As seen in §4.1, in the presence of negative electric potential, more electron may be trapped by the local magnetic mirror outside the torus, which may play an important role to the stability of ballooning mode. As in previous sections, we assume constant characteristic frequencies: ω_D, ω^* and ν_e , and consider the incompressible regime, $\zeta_e \ll \zeta_i \ll 1$. Integrating the both sides of eq.(10) over the velocity space taking into account the trapped electrons, for which $k_\parallel v_\parallel$ in the denominator vanishes, we have the approximate form of the perturbed electron density,

$$n_e = \frac{eN}{T}\left\{\hat{\phi} - P_t \frac{\bar{\omega} - \omega_D - \omega^*}{\bar{\omega} - \omega_D + i\nu_{eff}}\hat{\phi} - (1 - P_t)\frac{\bar{\omega} - \omega_D - \omega^*}{ck_\parallel}\hat{A}_\parallel\right\} \tag{37}$$

where $\nu_{eff} = \nu_e/\varepsilon$. For the sake of simplicity, we neglect the trapped ion contribution. All previous results for ions, therefore, can be used in the same forms. Introducing eqs.(11) and (37) into the quasi-neutrality condition, $n_e = n_i$, a relation between ϕ and $A_\parallel$ similar to eq.(14) can be derived. Substitution of eq.(10) into eq.(16), neglecting the trapped electron contribution for the parallel current, yields another relation between ϕ and $A_\parallel$ similar to eq.(16), in which the trapped electron contribution may not be negligible when $e\Phi/T$ is not very small as discussed in the Appendix A. Combining these relation between ϕ and $A_\parallel$, we have for $b \ll 1$, an eigenmode equation

$$k_{\parallel}\left|\frac{ck_{\parallel}}{k_D}\right|^2 k_{\perp}\psi - \left|\left(\bar{\omega}+\omega_D-\omega_g+\omega^*\right)\left(\bar{\omega}+\omega_D-\omega_g\right)(1-b)+\left(\bar{\omega}-\omega_D-\omega^*\right)\left(\bar{\omega}-\omega_D+i\nu_e\right)(1-P_t)\right|$$
$$-\frac{1}{D_{es}}\left\{\left(\bar{\omega}+\omega_D-\omega_g+\omega^*\right)(1-b)+\left(\bar{\omega}-\omega_D-\omega^*\right)(1-P_t)\right\}^2\Big|\psi=0 \qquad (38)$$

From eq.(15), taking into account the trapped elecrtron effect, the electrostatic part of dispersion function, from eq.(15), is written by

$$D_{es}=2-P_t\frac{\bar{\omega}-\omega_D-\omega^*}{\bar{\omega}-\omega_D+i\nu_{eff}} \qquad (39)$$

Substitution of eq.(39) into eq.(38) and averaging over the extended poloidal angle yields the dispersion relation

$$\left\{2\left(\bar{\omega}-\omega_D+i\nu_{eff}\right)-P_t\left(\bar{\omega}-\omega_D-\omega^*\right)\right\}\left\{b\omega_A^2-\left(\bar{\omega}+\omega_D-\omega_g+\omega^*\right)\left(\bar{\omega}+\omega_D-\omega_g\right)(1-b)\right.$$
$$\left.-\left(\bar{\omega}-\omega_D-\omega^*\right)\left(\bar{\omega}-\omega_D+i\nu_e\right)(1-P_t)\right\}+\left(\bar{\omega}-\omega_D+i\nu_{eff}\right)\left\{\left(\bar{\omega}+\omega_D-\omega_g+\omega^*\right)(1-b)\right.$$
$$\left.+\left(\bar{\omega}-\omega_D-\omega^*\right)(1-P_t)\right\}^2=0, \qquad (40)$$

As shown in Appendix B, with respect to $\bar{\omega}$, eq.(40) is a cubic equation, which involves the Alfven branch, drift mode branch, and ballooning mode branch. We are here interested about the ballooning mode branch in the MHD regime: $\omega>>\omega^*,\omega_D,\nu_e$ and $b<<1$. In this case, eq.(40) with the help of Mathematica reduces to a quadratic equation

$$\bar{\omega}^2+\frac{i}{b}\left\{\left(1-\frac{3}{2}P_t\right)\nu_e+P_t\nu_{eff}\right\}\bar{\omega}-\omega_A^2+\frac{\omega_D}{b}\left\{(2-P_t)\omega^*+2(1-P_t)\omega_D\right\}$$
$$-\frac{i}{b}\left\{\omega^*\nu_{eff}P_t+\nu_e\left((1-3P_t)\omega^*+2\omega_D\right)\right\}=0 \qquad (41)$$

where the centrifugal force effect ω_g has been neglected for the sake

of simplicity to concentrate to the trapped electron effect first. In eq.(41), ν_e means the collision effect by passing electrons which was a cause of the resistive ballooning mode as seen in §3, while ν_{eff} represents the collision by trapped electrons, which was a cause of the electrostatic dissipative trapped electron mode as seen in §4.2.

The imaginary coefficient of $\bar{\omega}$ (the second term) represents the collision damping as seen in §3, which reduces the growth rate. However, it does not make the growth rate negative. Since $\nu_e \ll \nu_{eff}$, terms with ν_e in eq.(41) may be neglected as compared to those terms with ν_{eff}. In this case, by solving eq.(41), we have

$$\bar{\omega} = -i\frac{P_t \nu_{eff}}{2b} \pm \left[\omega_A^2 - \left(\frac{P_t \nu_{eff}}{2b} \right)^2 - \left\{ \frac{\omega_D}{b} \left((2-P_t)\omega^* + 2(1-P_t)\omega_D \right) \right\} + i\frac{P_t \nu_{eff}}{b} \omega^* \right]^{\frac{1}{2}} \qquad (42)$$

The first term in eq.(42) represents the collision damping, i.e., it reduces the growth rate, but does not change the stable β-region as discussed in § 3. Without collision effect, $\nu_{eff}=0$, eq.(42) reduces to the ideal mode growth rate which still has the trapped electron effect in P_t in the sense that the passing particle effect is reduced by P_t. This growth rate is calculated as shown in Fig.9. One will see the increase of electron trapping rate P_t stabilizes the ideal ballooning mode as seen in Fig.9.

Whether the last imaginary term in the square root in eq.(42) makes the growth rate negative or positive must be examined. We express the growth rate of eq.(42) in the form

$$\gamma = -\frac{P_t \nu_{eff}}{2b} + |S|^{\frac{1}{2}} \sin\frac{\vartheta}{2} \qquad (43)$$

where S is the complex quantity in the square root in eq.(42) and the angle ϑ is defined by $\vartheta=\tan^{-1}(\mathrm{ImS}/\mathrm{ReS})$. For the sake of simplicity, we consider eq.(43) at the ideal marginal stability state:

$$\omega_A^2=\left\{\frac{\omega_D}{b}\left(2-P_t\right)\omega^*+2\left(1-P_t\right)\omega_D\right\} \tag{44}$$

In this case, $\gamma=0$ when ImS=0. When ImS$\neq$0, ϑ must be in the range $\pi/2<\vartheta<\pi$. The maximum value $\sin(\pi/2)=1$ is attained when ImS$\cong$0. Expanding in power of ImS in Taylor series, we find the growth rate γ is positive: $\gamma=(\mathrm{ImS})^2/8(\mathrm{ReS})^3>0$ for ReS>0. This means that the trapped electrons destabilezes the ballooning mode at the marginal stability state. This can also be seen by numerical results in Fig. 10, where the normalized growth rate is plotted versus β for different values of P_t and ν_{eff}.

§5.Energetic Particle Effect

In high temperature plasmas, energetic ions may be produced by auxiliary heating such as neutral beam injection and RF-heating. In fusion plasmas, α-particles are also produced. These energetic particles may interact with the bulk plasma, and some time excites or stabilizes various modes.

In this section, we consider the effect of these energetic ions on the ballooning mode by the same kinetic approach employed in the previous sections assuming that energetic particles are collisionless and described by the Maxwellian distribution. In this case, energetic ions can be treated by the same manner as the back ground plasma. The perturbed distribution can be written by

$$\hat{f}_h = -\frac{e}{T} f_{oh}\left[\hat{\phi} - J_0^2(a_h)\frac{\bar{\omega} - \omega_{Dh} - \omega_{gh} - \omega^*}{\bar{\omega} - \omega_{Dh} - \omega_{gh} - k_\parallel v_\parallel}\left(\hat{\phi} - \frac{v_\parallel}{c}\hat{A}_\parallel\right)\right] \tag{45}$$

where all characteristic quantities for energetic ions are expressed by the suffix h. The quantity $k_\parallel v_\parallel$ in the denominator in eq.(45) is absent for trapped particles. Making use of the Maxwell distribution (2) for f_{oh}, and integrating eq.(45) over the velocity space neglecting trapped particles, we have the perturbed density

$$n_h = -\frac{e_h N_h}{T_h}\left[\hat{\phi} + \frac{\bar{\omega} - \omega_{Dh} - \omega_{gh} - \omega^*_h}{k_\parallel v_\parallel}\Gamma_o(b_h)\left\{Z_o(\zeta_h)\hat{\phi} - Z_1(\zeta_h)\frac{v_h}{c}\hat{A}_\parallel\right\}\right] \tag{46}$$

where $\zeta_h = (\omega - \omega_{Dh} - \omega_{gh})/k_\parallel v_h$.

Substitution of eq.(46) into the quasi-neutrality condition yields a relation between ϕ and $A_\parallel$ similar to eq.(4). Introducing eq.(45) into the Ampere law neglecting the trapped particle contribution to the parallel current, we have another relation similar to eq.(7). Combining these relations, we obtain the eigenmode equation including the energetic particle effect in the form

$$\begin{aligned} k_\perp^2\left|\frac{ck_\perp}{k_D}\right|^2 k_\parallel^2\psi - \Big|\Big\{ &(\bar{\omega} + \omega_D - \omega_g + \omega^*)(\bar{\omega} + \omega_D - \omega_g) Z_1(\zeta_i)\Gamma_o(b) + (\bar{\omega} - \omega_D - \omega^*)(\bar{\omega} - \omega_D) Z_1(\zeta_e) \\ &+ c_h(\bar{\omega} - \omega_{Dh} - \omega_{gh} - \omega^*_h)(\bar{\omega} - \omega_{Dh}) Z_1(\zeta_h)\Gamma_o(\zeta_h) - \frac{1}{D_{es}}\Big\{(\bar{\omega} + \omega_D - \omega_g + \omega^*) Z_1(\zeta_i)\Gamma_o(b) \\ &+ (\bar{\omega} - \omega_D - \omega^*) Z_1(\zeta_e) + c_h(\bar{\omega} - \omega_{Dh} - \omega_{gh} - \omega^*_h) Z_1(\zeta_h)\Gamma_o(\zeta_h)\Big\}^2\Big|\psi = 0 \end{aligned} \tag{47}$$

where $c_h = (e_h/e)^2 (N_h/N)(T/T_h) = (k_{Dh}/k_D)^2$. The electrostatic part of the dispersion function D_{es} is also given in the similar form as eq.(15). However, it may change significantly depending on the model and assumptions we employ.

For energetic particles, we assume $\omega^*_h = \omega^* T_h/T$ and $\omega_{Dh} = \omega_D T_h/T >>$

$\omega \cong \omega_A$. The centrifugal force drift frequency $\omega_{gh}=v_E^2/2r\Omega_h = \omega_g e_h M_h/eM_i \cong \omega_g$ is independent of energy, and may be neglected as compared with ω_{Dh}. If we assume $\omega^* \cong 10$ KHz, $T_h/T=700$ for T=5 KeV and $T_h=3.5$ MeV for α-particles, then $\omega_{Dh}=e_n\omega^* T_h/T \cong 1.4$ MHz, and $v_h \cong 1.3\times10^9$ cm/sec. The transit frequency becomes $\omega_{th}=k_{\|}v_h \cong 0.52$ MHz for R=200 cm and q=2. The Alfven frequency $\omega_A \cong 30$ KHz for $\beta=0.01$.

Without the plasma rotation, ω_D in ζ_h is absent. In this case, $|\zeta_h| \ll 1$ as in the bulk plasma. Including the collisionless trapped particles contribution, the perturbed density may approximately be written by

$$n_h = -\frac{e_h N_h}{T_h}\left[\hat{\phi} + \frac{\bar{\omega}-\omega_{Dh}-\omega^*_h}{k_{\|}v_{\|}}\Gamma_o(b_h)\,(1-\sqrt{\varepsilon_T})\,\frac{\hat{A}_{\|}}{ck_{\|}} - \left\langle \frac{\bar{\omega}-\omega_{Dh}-\omega^*_h}{\bar{\omega}-\omega_{Dh}} \right\rangle_T \hat{\phi}\right] \qquad (48)$$

where $\langle\ \rangle_T$ means the velocity space integration for trapped particles.

In the rotating plasmas, however, ζ_h has ω_{Dh} in the numerator as defined in the above, and the criterion change to $|\zeta_h| \gg 1$. In this case, since $Z_o(\zeta) = -(1+1/2\zeta^2)/\zeta$ for $|\zeta| \gg 1$, the perturbed density may be approximated by

$$n_h = -\frac{e_h N_h}{T_h}\left[\hat{\phi} - \frac{\bar{\omega}-\omega_{Dh}-\omega^*_h}{\bar{\omega}-\omega_{Dh}}\Gamma_o(b_h)\,(1-\sqrt{\varepsilon_T})\,\hat{\phi} - \left\langle \frac{\bar{\omega}-\omega_{Dh}-\omega^*_h}{\bar{\omega}-\omega_{Dh}} \right\rangle_T \hat{\phi}\right] \qquad (49)$$

When ω_{Dh} and ω^*_h are constants, the trapped particle contribution is canceled out in eq.(49). Making use of the approximation (49), the electrostatic dispersion function may be approximated by

$$D_{es} = 2 - c_h \frac{\bar{\omega}-\omega_{Dh}-\omega^*_h}{\bar{\omega}-\omega_{Dh}}\Gamma_o(b_h) \qquad (50)$$

which has no trapped particle effect. Introducing eq.(50) into eq.(47), and applying the condition $|\zeta|>>1$ for the bulk plasma, we have

$$\left(2-c_h\frac{\bar{\omega}-\omega_{Dh}-\omega^*_h}{\bar{\omega}-\omega_{Dh}}\Gamma_0(b_h)\right)\left\{b\omega_A^2-(\bar{\omega}+\omega_D-\omega_g+\omega^*)(\bar{\omega}+\omega_D-\omega_g)(1-b)-(\bar{\omega}-\omega_D-\omega^*)(\bar{\omega}-\omega_D)\right.$$
$$\left.+\frac{1}{2}c_h\frac{\omega-\omega_{Dh}-\omega^*_h}{\omega-\omega_{Dh}}\Gamma_0(b_h)\omega_{th}^2\right\}+\left\{(\bar{\omega}+\omega_D-\omega_g+\omega^*)(1-b)+\bar{\omega}-\omega_D-\omega^*\right\}^2=0 \qquad (51)$$

In general, eq.(51) is the fourth order algebraic equation with respect to $\bar{\omega}$, and very complicated to solve analytically.

We solve eq.(51) by assuming $\omega<<\omega_{Dh}$. In this case, the energetic particle contribution can be approximated as $(\omega-\omega_{Dh}-\omega^*_h)/(\omega-\omega_{Dh})=\omega^*_h/\omega_{Dh}=\omega^*/\omega_D$, and eq.(51) can be reduced to the quadratic equation

$$(b-2c_h)\bar{\omega}^2+\left\{b(\omega^*-\omega_g)+2c_h\omega_g\right\}\omega+2(\omega^*+\omega_D-\frac{1}{2}\omega_g)-b\omega_A^2-2c_h\omega_{th}^2=0 \qquad (52)$$

which can easily solved. The imaginary part of the solution ω or the growth rate becomes

$$\gamma=\frac{1}{2(b-2c_h)}\left[4(b-2c_h)\left\{2\left(\omega^*+\omega_D-\frac{\omega_g}{2}\right)\left(\omega_D-\frac{\omega_g}{2}\right)-b\omega_A^2-2c_h\omega_{th}^2\right\}-\left\{b(\omega^*-\omega_g)+2c_h\omega_g\right\}^2\right]^{\frac{1}{2}} \qquad (53)$$

In the limits $C_h\to 0$ and $\omega_g\to 0$, eq.(53) reduces to the drift ballooning mode growth rate given by eq.(24). As seen in eq.(53), the energetic particle contribution $C_h\omega_{th}^2$ is always stabilizing the ballooning mode.

The sufficient condition for the stability can be written by

$$\frac{1}{2}\Gamma_o(b_h)\,C_h\omega_{th}^2 \geq \frac{\omega_D}{\omega^*}\left\{(\omega^*+\omega_D-\frac{1}{2}\omega_g)(\omega_D-\frac{1}{2}\omega_g)-\frac{b}{2}\omega_A^2\right\} \qquad (54)$$

The right hand side of inequality (54), which is the ideal MHD quantity Q is plotted as a function of β in Fig.11 for different values of ω_g. As seen in Fig.11, there is a maximum Q_{max}. The energetic particles can completely stabilize the ballooning mode when $C_h\omega_{th}^2 > Q_{max}$. Since $\Gamma_o(b_h)\,(k_{Dh}/k_D)^2 \cong 10^{-4}$ and $(\omega_{th}/\omega^*)^2 \cong 3\times10^3$ for α-particles, the energetic particle contribution $Ch(\omega_{th}/\omega^*)^2 \cong 0.3$ can be larger than Q at least in certain regions of β. Since Q decreases verly slowly in the high-β region, the small increase of the energetic particle contribution $Ch(\omega_{th}/\omega^*)^2$ enlarges the second stability region significantly.

The growth rate given by eq.(53) is plotted as a function of β for different values of C_h and ω_g in Fig.12. The centrifugal force due to plasma rotation ω_g always destabilizes the ballooning mode. It not only enlarges the growth rate but also expands the unstable β-region. The energetic particle stabilization can overcome this destabilization particularly in the high-β region, and reduces the second stability boundary significantly as seen in Fig.12. In the higher-β region, another unstable region appears. This instability is induced from the drift reversal of energetic particle, i.e., the change sign of ω_{Dh} in C_h. This unstable region may correspond to the one reported in Ref.(14)..

§6. Effect of Fluid Flow Shear

In previous sections, we investigated the effect of plasma rotation on ballooning modes without taking into account the radial variation of the plasma rotation frequency ω_E, i.e., we assumed the rigid rotator model. In this section, we consider briefly the effect of the fluid flow shear on the ideal ballooning mode.

When the fluid flow has shear, the eikonal S of perturbations depends on time[6]. It is expressed in the toroidal coordinate system (q,θ,ζ) from the flow resonant condition $dS/dt=0$ in the form

$$S=n\left(\zeta-\theta q-\Omega t+\int_{q_0}^{q} q(\theta')\,d\theta'\right) \tag{55}$$

The perpendicular wave number in this case is also time dependent:

$$\mathbf{k}_\perp=\nabla S=n\left(\nabla\zeta-q\nabla\theta-(\theta+\dot{\Omega}t-\theta_0)\nabla q\right) \tag{56}$$

where $\dot{\Omega}=d\Omega/dq$. The time dependence through $\dot{\Omega}t$ is only in $\mathbf{k}_\perp$. The time dependence appears no other place. In this case, the average can be approximated by

$$\left\langle k_\perp^2\right\rangle=k_\theta^2\left(1+s^2\left(\frac{\pi^2}{3}-2.5\right)-\frac{10}{9}\alpha s+\frac{5}{12}\alpha^2+s^2\theta_1^2\right) \tag{57}$$

where $\theta_1=\dot{\Omega}t-\theta_0$.

In the ideal case, the dispersion relation may be written in the form

$$\left(\omega-m\Omega(q)+i\gamma\right)\psi=i\Lambda\psi \tag{58}$$

where $\omega_E=m\Omega(q)$ and $\Lambda=(2\omega_*\omega_D/b(\theta_1)-\omega_A^2)^{1/2}$. From the definition of $b=\langle k_\perp^2\rangle\rho^2/2$ and eq.(57), Λ depends on time through θ_1. In the zeroth order, eq.(58) yields $\omega=m\Omega(q_0)$ which represents the flow resonant condition. In the first order, eq.(58) may be written by

$$\left(\gamma+\dot{\Omega}\frac{\partial}{\partial\theta_1}\right)\psi=\Lambda\psi \tag{59}$$

The solution of eq.(59) is given in the form

$$\psi(\theta)=\psi_0\exp\left(\int_{\theta_0}^{\theta}\frac{\gamma-\Lambda}{\dot{\Omega}}d\theta'\right) \tag{60}$$

If we require the periodicity to eq.(60), the growth rate may be

approximated by

$$\gamma = \frac{1}{\theta^*}\int_0^{\theta^*} \Lambda d\theta' \qquad (61)$$

where θ^* is the boundary value above which Λ becomes imaginary.

Variation of Λ versus θ_1 is plotted in Fig.13 for different values of the magnetic shear parameter s. Without flow shear, $\dot{\Omega}=0$, the growth rate is given by Λ at $\theta_1=0$. With flow shear, $\dot{\Omega}\neq 0$, the growth rate given by eq.(61) is plotted versus s in Fig.14 for $\beta=0.05$. The growth rate without shear is also plotted for comparison. Since the flow shear always reduces the growth rate, the flow shear stabilizes the ideal ballooning mode particurarly in the larger shear parameter s region.

The averaged growth rate given by eq.(61) has no $\dot{\Omega}$, it is independent of the flow shear parameter $\dot{\Omega}$. The growth rate γ has the discontinuity at $\dot{\Omega}=0$, i.e., with and without the fluid flow shear physics may be different as discussed in Refs.(7) and (8).

§7. Summary and Discussion

A kinetic approach is developed to study the stability of electromagnetic low frequency modes in rotating Maxwellian plasmas. The theory is applied to the long wave length MHD modes, and the growth rates are derived in simple analytical forms in the rigid rotator model for the cases of ideal and resistive ballooning modes.

The plasma rotation due to the radial electric field makes the Doppler shift in the laboratory system, which directly does not affect the stability. The centrifugal force due to the plasma rotation, however, strongly destabilizes the ballooning modes particularly when the flow velocity is close to the sound velocity, i.e., the Mach number is close to unity.

The electron collision on the one hand stabilizes the long wave

modes by the collision damping. On the other hand, it destabilizes the resistive ballooning mode in the high-β region.

When the fluid flow shear effect is taken into account, the discontinuity in the growth rate occurs, which may indicate the physical difference between the rigid rotator and shear flow models. With the flow shear, the ballooning mode growth rate is reduced particurarly in the larger magnetic shear regions.

Although the plasma rotation strongly destabilizes the ballooning modes, when energetic particles such as energetic ions and α-particles exist, they are effective to stabilize and overcome the destabilization particularly in the high-β region. The second stability boundary may be reduced by the energetic particles.

The electric potential Φ induced by the radial electric field changes the particle trapping condition in the velocity space. For $e\Phi>0$, the particle trapping rate is increased particurarly for $e\Phi/T\simeq 1$. In this case almost 90% of particles are trapped by the electromagnetic potential. When $\Phi<0$ as in tokamaks, the electron trapping rate is increased, which may strongly destabilize the dissipative trapped electron mode.

Our theory is not completely consistent in the sense that the curvature drift frequency ω_D which is the source of ballooning mode is introduced in the simple form through the radial gravity G given by eq.(4). The averaged curvature drift frequency $\langle\omega_D\rangle$ in §4, however, is calculated making use of general curvature velocity $\mathbf{v}_d=\mathbf{b}\times(v_\perp^2\ \nabla\ln B/2+\ v_\parallel^2\kappa)$. To be consistent the gyrokinetic solution must be derived for the general drift velocity. The validity of using the simple strong ballooning mode trial function in calculations of the average for all cases should be examined.

Although we have assumed that the radial electric field is given, it should be determined by transport processes and momentum balance condition. As discussed briefly in Appendix C, if the anomalous

electron transport is dominant, the rotation frequency ω_E is related to the electron diamagnetic drift frequency ω^*. Applicability of this should also be examined.

Acknowledgement

The author would like to thank to Prof. A.Hirose for helpful comments to this study. He is grateful to Prof. M. Wakatani and Dr. H. Sanuki for enlightening conversations. The acknowledgement is also due to Prof. T.Amano for providing information of Mathematica. This study was a joint research program with National Institute for Fusion Science.

Appendix A. Effect of Electric Potential on Plasma Dispersion Function

In the calculation of the parallel electron current in the Ampere' law, the trapped electron effect was only taken into account approximately by $(1-P_t)$ in the passing electron velocity integral. Precisely, the velocity integral of the propagator for passing electron for $e\Phi>0$ is calculated as follows:

$$G_p(\zeta) = -\int \frac{\omega v_t^p f_0}{\omega - k_t v_t + i\nu_e} d^3v$$

$$= \frac{\omega}{k_t v_t}\left[\hat{Z}_p\left(\zeta, \sqrt{\frac{e\Phi}{T}}\right) - \exp\left(\frac{e\Phi}{\varepsilon T}\right)\hat{Z}_p\left(\zeta, \sqrt{\frac{e\Phi}{T}}\right)\right] \qquad (A.1)$$

where Zp is the moment integral of the plasma dispersion function in which the trapped particle effect is deleted:

$$\hat{Z}_p(\zeta,\delta) = \frac{1}{\sqrt{\pi}}\left(\int_0^{+\infty} + \int_{-\infty}^{-\delta}\right)\frac{u^p e^{-u^2} du}{u-\zeta} \qquad (A.2)$$

The trapped electron contribution in the parallel current does not vanish:

$$\frac{\hat{A}_1}{c}\int_T \frac{\omega-\omega_D-\omega^*}{\omega-\omega_D+i\nu_{eff}} v_\parallel^2 f_0 d^3v = \frac{\hat{A}_1}{c}\frac{\omega-\omega_D-\omega^*}{\omega-\omega_D+i\nu_{eff}} I_2 \qquad (A.3)$$

By transforming variavles $x=v_\parallel/v_e$ and $y=v_\perp/v_e$, the second moment integral can be calculated as follows:

$$I_2 = \int_T v_\parallel^2 f_0 d^3v = \frac{4N}{\sqrt{\pi}} v_e^2 \int_0^\infty dx x e^{-x^2} \int_0^{\sqrt{x^2+e\Phi/T}} dy y^2 e^{-y^2}$$

$$= Nv_e^2\left[\frac{1}{2}\mathrm{erf}\left(\sqrt{\frac{e\Phi}{T}}\right) - \frac{1}{\sqrt{\pi}}\sqrt{\frac{e\Phi}{T}}e^{-\frac{e\Phi}{T}} + \varepsilon_T^{\frac{3}{2}}\left\{\frac{1}{\sqrt{\pi}}\sqrt{\frac{e\Phi}{T}} + \frac{1}{2}\left(1-\mathrm{erf}\left(\sqrt{\frac{e\Phi}{T}}\right)\right)e^{\frac{e\Phi}{\varepsilon_T T}}\right\}\right] \qquad (A.4)$$

where erf(z) is the error function defined by

$$\mathrm{erf}(z) = \frac{2}{\sqrt{\pi}}\int_0^z du e^{-u^2}$$

In the derivation of eq.(A.4), the partial integrations have been used. For $e\phi/T<<1$, eq.(A.4) is approximated by

$$I_2 = Nv_e^2\left(\frac{e\Phi}{T} + \frac{1}{2}\varepsilon_T^{\frac{3}{2}}\right)$$

When $e\Phi/T=1$, which is experimentally observed, the contribution from eq.(A.3) for $k_\parallel v_e >> \omega$ may play an important contribution to the parallel current.

Appendix B. Cubic Dispersion Equation

When we expand eq.(40) by using Mathematica, we have in total 134 terms, which consists of three ω^3, 15 ω^2, 44 ω and 72 ω^0 terms, respectively. This is too long to handle. We neglect b^2, bP_t $b\omega_D^2$ and ω_D^3 terms, and also only ν_{eff} terms are taken into account neglecting

ν_e terms. In this case, eq.(40) is reduced to a cubic equation

$$-2b\bar{\omega}^3+2\left\{b(\omega_D+\omega_g-\omega^*)-i\nu_{eff}(P_t+b-P_t^2)\right\}\bar{\omega}^2+2\Big[b\omega_A^2-(\omega_D-\frac{\omega_g}{2})\left\{2(1-P_t)(\omega_D-\frac{\omega_g}{2})-\omega^*(2-P_t)\right\}$$

$$+i\nu_{eff}\left\{P_t(\omega^*+\omega_g-P_t\omega^*)+b(\omega_g-\omega^*)\right\}\Big]\bar{\omega}-2\omega_A^2\omega_D-4(1-P_t)\omega_D^2\omega_g+(1-P_t)\omega_D\omega_g^2+4\omega_D^2\omega^*-6P_t\omega_D^2\omega^*$$

$$+(5P_t-2)\omega_D\omega_g\omega^*-P_t\omega_g^2\omega^*-2P_t\omega_D\omega^{*2}+P_t\omega_g\omega^{*2}+2i\nu_{eff}\Big\{b\omega_A^2-2\omega_D^2+P_t\omega_D^2+(2-b)\omega_D\omega_g$$

$$-\frac{\omega_g^2}{2}+(P_t-2)\omega_D\omega^*+b\omega_D\omega^*+(1-P_t)\omega_g\omega^*+\frac{1}{2}P_t^2(\omega_D+\omega^*)^2\Big\}=0$$

This equation is still complicated. We consider the low-β MHD regime: $\omega\cong\omega_A>>\omega^*>\omega_D$. In this case, the zeroth order terms may be neglected, and we have a simpler quadratic equation

$$-b\bar{\omega}^2+\left\{b(\omega_D+\omega_g-\omega^*)-i\nu_{eff}(P_t+b-P_t^2)\right\}\bar{\omega}+\Big[b\omega_A^2-(\omega_D-\frac{\omega_g}{2})\left\{2(1-P_t)(\omega_D-\frac{\omega_g}{2})-\omega^*(2-P_t)\right\}$$

$$+i\nu_{eff}\left\{P_t(\omega^*+\omega_g-P_t\omega^*)+b(\omega_g-\omega^*)\right\}\Big]=0$$

Appendix C. Ambipolar Condition

When the momentun balance condition is ignored, the radial electric field may be determined from the ambipolar condition:

$$\Gamma_\perp^e-\Gamma_\perp^i=0$$

where $\Gamma_\perp=-D_\perp\nabla_\perp N$ is plasma particle flux. If we assume an anomaluos transport state in which the electron flux may be much larger than the ion flux: $|\Gamma_\perp^e|>>|\Gamma_\perp^i|$. In this case, the ambipolar condition may be written in the form

$$\Gamma_\perp^e=-D_\perp^eN'+m_eNE_r\cong0$$

where m_e is electron mobility. From the Einstein relation: $m_e=-eD_\perp^e/T$, and the above ambipolar condition, we have

$$E_r=-\frac{T}{e}\frac{N'}{N}$$

which can be rewritten in the form

$$\frac{d\Phi}{dr}=\frac{T}{e}\frac{d}{dr}\ln N$$

In terms of velocities, this condition can also be written as

$$v_E=\frac{cE_r}{B}=-\frac{ct}{eB}\frac{N'}{N}=-v_d$$

i.e., the flow velocity v_E is equivalent to the opposite of diamagnetic electron drift velocity v_d. In terms of frequencies, this can be written as $\omega_E=-\omega^*$.

References

1) R.J.Groebner,K.H.Burrel,and R.P.Seraydarian:Phys.Rev.Lett., **64**(1990)3015.

2) G.A.Hallock,J.Mathew,W.C.Jennings,et al.:Phys.Rev.Lett.,**56**(1986) 1248.

3) H.Sanuki,K. Itoh,K.Ida and S-I.Itoh:J.Phys.Soc.Jpn.**60**(1991)3698.

4) E.Hameiri and P.Laurence:J.Math.Phys. **25**(1984)396.

5) E.Hameiri and S.T.Chun:Physical Review A,**41**(1990)1186.

6) W.A.Cooper:Plasma Phys.Controlled Fusion **30**(1988)1805.

7) A.Bhattacharjee,R.Icaono et al.:Phys.Fluids **B1**(1989)2207.

8) F.L.Waelbroeck and L.Chen:Phys.Fluids **B3**(1991)601.

9) E.J.Doyle,R.J.Groebner,K.H.Burrel, et al.:Phys.Fluids **B3** (1991)2300.

10) K.Miyamoto, Introduction to Plasma Physics for Fusion, Iwanami, 1976.

11) T.Yamagishi:J.Phys.Soc.Jpn. **57**(1988)2730.

12) S.Wolfram:Mathematica, A system for Doing Mathematics by Computer (Addison-Wesely Publishing Co., New York, 1988).

13) A.Hirose:Phys. Fluids,**B3**(1991)1125

14) X.H.Wang,A.Bhattacharjee,M.E.Mauel and J.W.Van Dam:Phys.Fluids,**31** (1988)332.

Figures Captions

Fig.1 :Variation of normalized ideal ballooning mode growth rate γ/ω^* versus β and s presented by surface graphics for $\omega_g=0$, $e_n=0.2$ and $q=2$.

Fig.2 :Variation of normalized ideal ballooning mode growth rate γ/ω^* versus β for different values of plasma rotation frequency ω_g for $s=1$.

Fig.3 :Variation of normalized growth rate γ/ω^* versus β for different collision frequency ν_e for $s=1$.

Fig.4 :Surface graphics of normalized resistive ballooning mode growth rate for $\nu_e/\omega^*=0.6$ and $\omega_g=0$.

Fig.5:Illustration of variation of v as a function of poloidal angle θ.

Fig.6:Illustration of "loss cone" boundary in velocity space in the presence of different signs of electric potential Φ.

Fig.7:Variation of particle trapping rate versus b and s presented by surface graphics for $e\Phi>0$.

Fig.8:Variation of normalized dissipative trapped electron mode growth rate γ/ω^* versus $e\Phi/T$ for $\nu_{eff}/\omega^*=0.5$ and different values of b.

Fig.9:Variation of normalized ideal ballooning mode growth rate γ/ω^* versus β for different values of electron trapping rate P_t and $\nu_{eff}=0$.

Fig.10:Variation of normalized ballooning mode growth rate γ/ω^* versus β for different values of ν_{eff} and P_t.

Fig.11.:Variation of Q as a function of β for different values of ω_g.

Fig.12:Variation of normalized growth rate γ/ω^* versus β for $s=1$ and different values of energetic particle contribution c_h and ω_g Curve a represents the ideal case $\omega_g=0$, and $c_h=0$, Cuve b : $\omega_g/\omega^*=-0.5$, and $c_h=0$, Curve c:$\omega_g/\omega^*=-0.5$, and $c_h=0.0003$.

Fig.13:Variation of Λ as a function of θ_1 for different values of s.

Fig.14:Variations of normalized ideal ballooning mode growth rates γ/ω^* versus s with fluid flow shear(solid curve) and without flow shear(broken curve) for $\beta=0.05$.

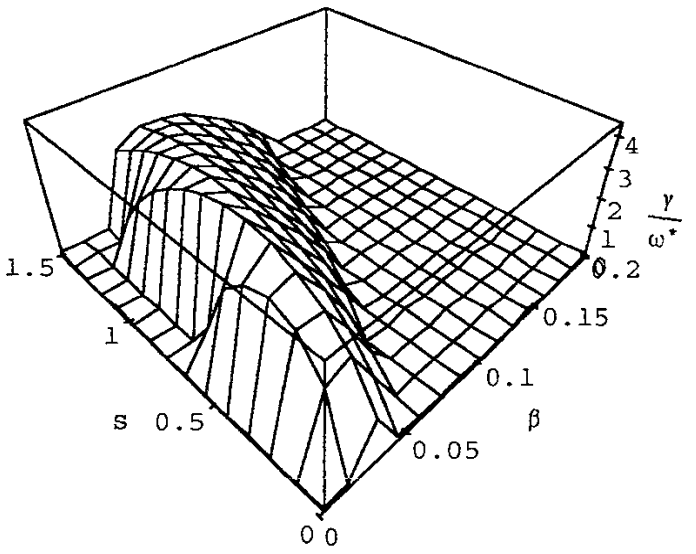
4
3
2
1
γ/ω*
1.5
1
s 0.5
0 0
0.05
0.1
β
0.15
0.2

Fig.1

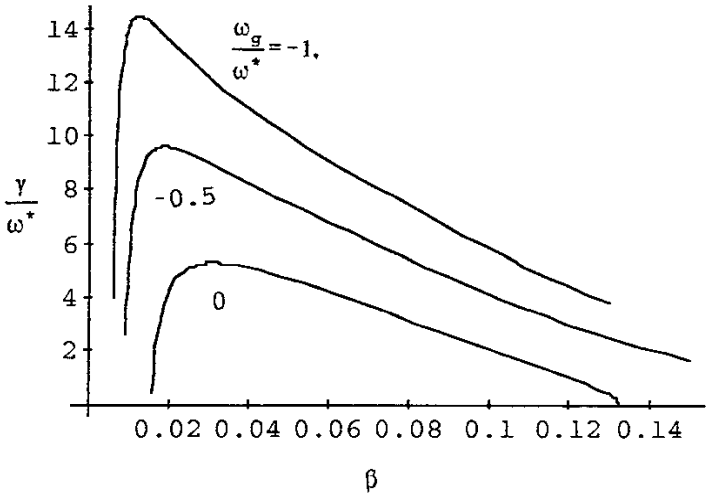
14
12
10
8
6
4
2
γ/ω*
ω_g/ω* = -1.
-0.5
0
0.02 0.04 0.06 0.08 0.1 0.12 0.14
β

Fig.2

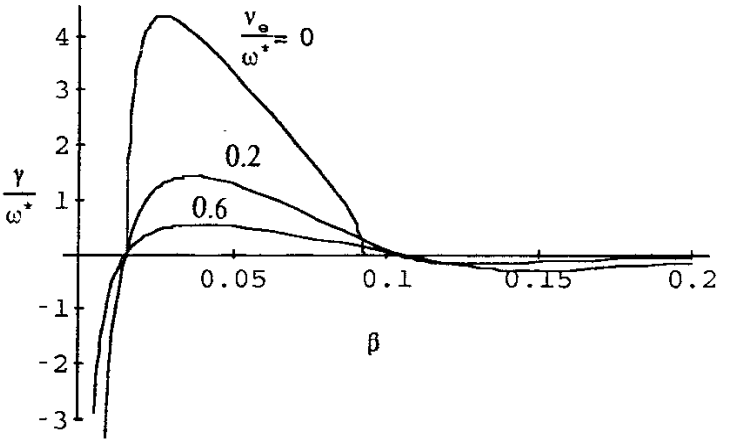
$\frac{\nu_e}{\omega^*} = 0$
0.2
0.6
$\frac{\gamma}{\omega^*}$
4
3
2
1
-1
-2
-3
0.05
0.1
0.15
0.2
β

Fig.3

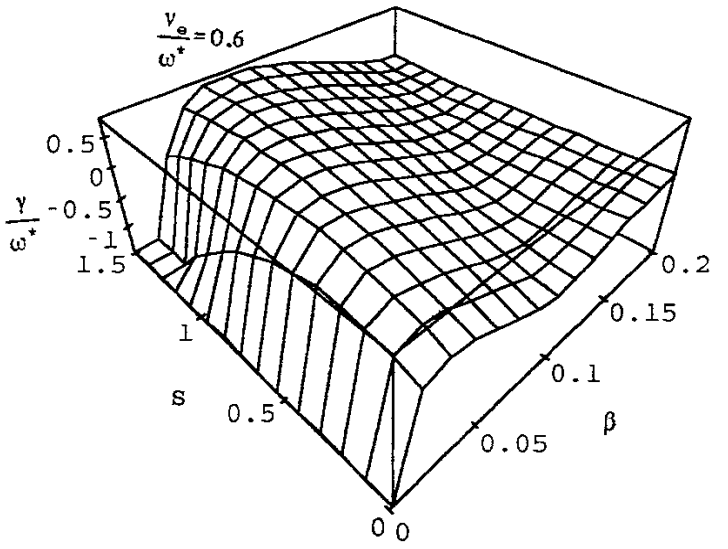
$\frac{\nu_e}{\omega^*} = 0.6$
$\frac{\gamma}{\omega^*}$
0.5
0
-0.5
-1
1.5
1
s
0.5
0
0
0.05
0.1
0.15
0.2
β

Fig.4

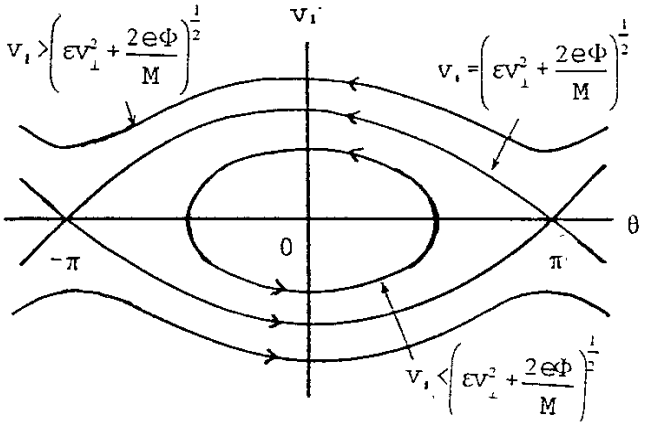
$v_\parallel$
$v_\parallel > \left(\varepsilon v_\perp^2 + \frac{2e\Phi}{M}\right)^{\frac{1}{2}}$
$v_\parallel = \left(\varepsilon v_\perp^2 + \frac{2e\Phi}{M}\right)^{\frac{1}{2}}$
$v_\parallel < \left(\varepsilon v_\perp^2 + \frac{2e\Phi}{M}\right)^{\frac{1}{2}}$
θ
$-\pi$
0
π

Fig.5

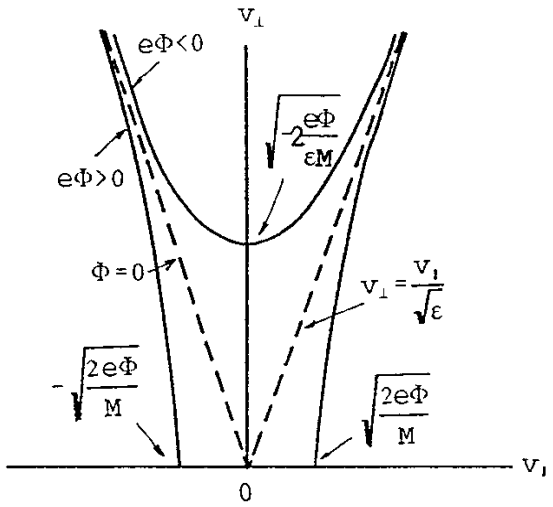
$v_\perp$
$e\Phi<0$
$e\Phi>0$
$\sqrt{-2\frac{e\Phi}{\varepsilon M}}$
$\Phi=0$
$v_\perp = \frac{v_\parallel}{\sqrt{\varepsilon}}$
$-\sqrt{\frac{2e\Phi}{M}}$
$\sqrt{\frac{2e\Phi}{M}}$
$v_\parallel$
0

Fig.6

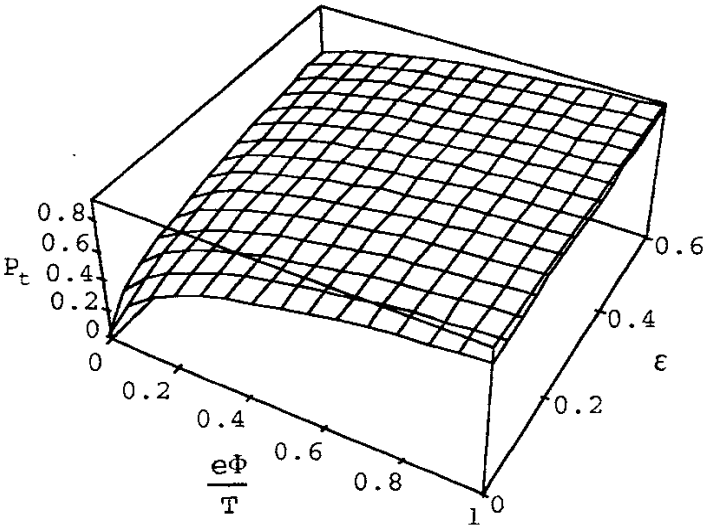
0.8
0.6
P_t 0.4
0.2
0
0
0.2
0.4
0.6
0.8
1
$\frac{e\Phi}{T}$
0
0.2
0.4
0.6
ε

Fig.7

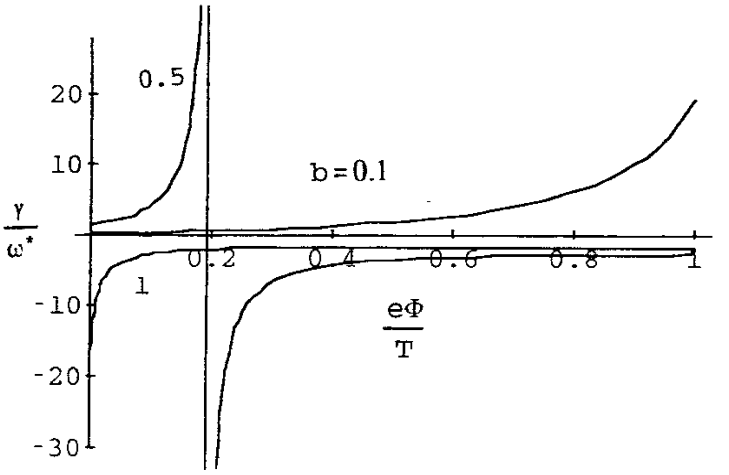
20
10
-10
-20
-30
0.5
1
b=0.1
$\frac{\gamma}{\omega^*}$
0.2
0.4
0.6
0.8
1
$\frac{e\Phi}{T}$

Fig.8

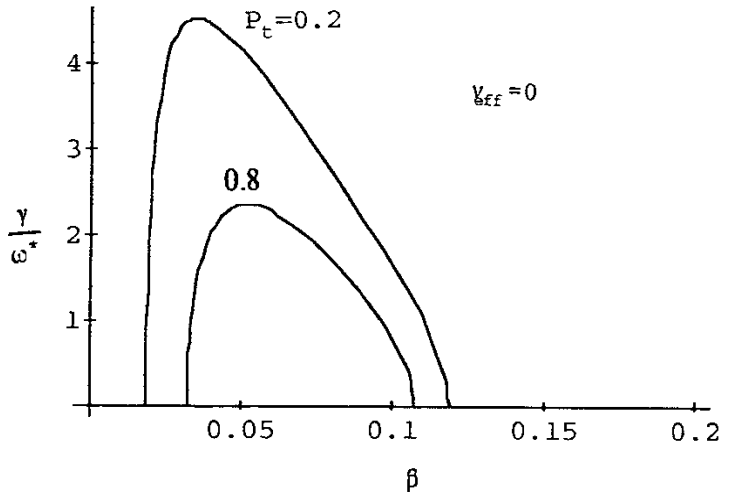

Fig.9

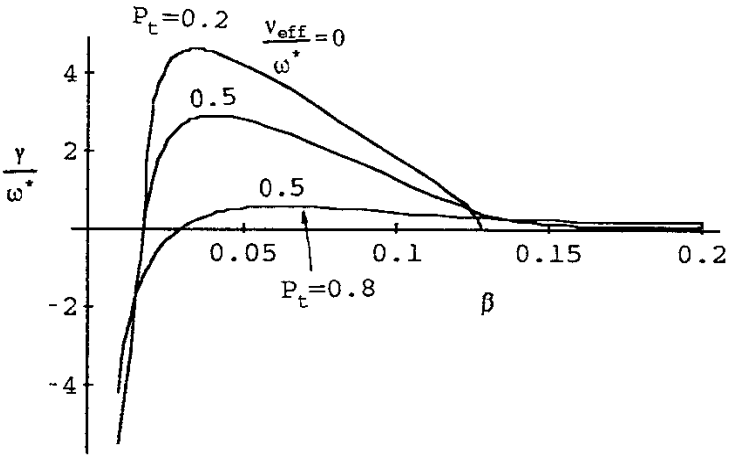

Fig.10

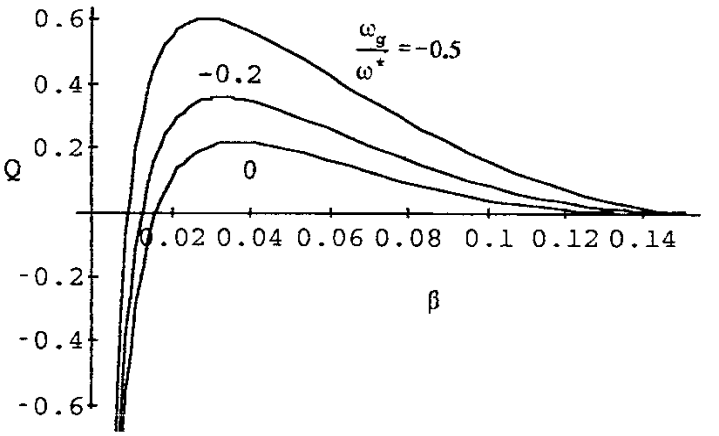

Fig.11

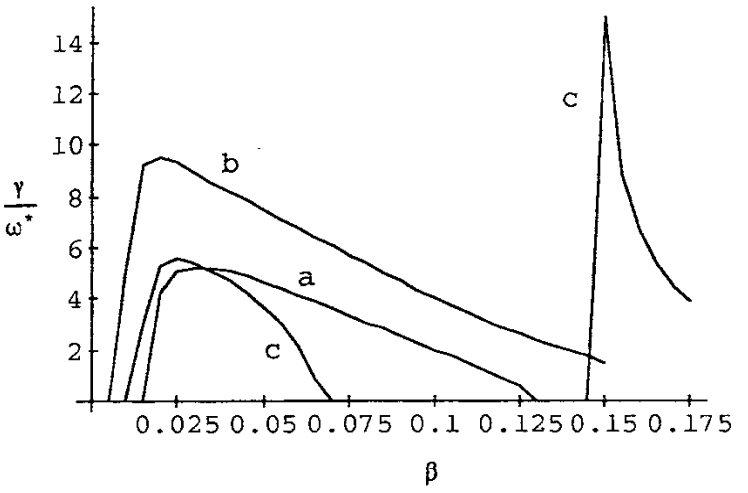

Fig.12

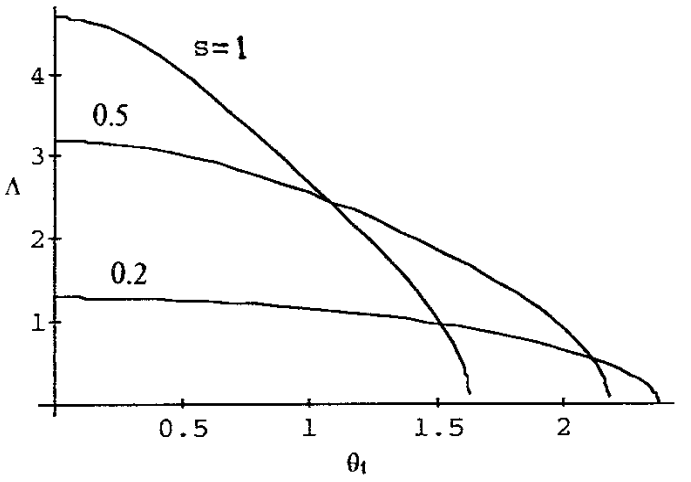

Fig.13

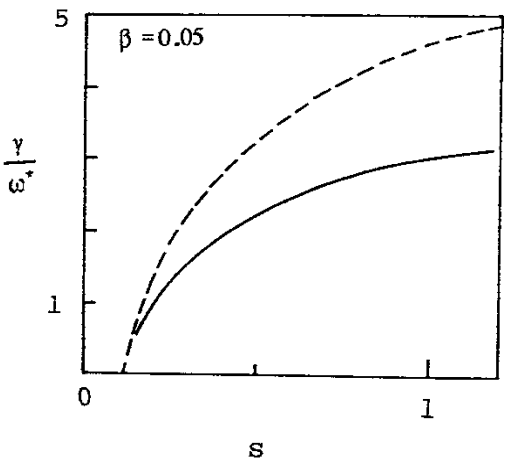

Fig.14

Recent Issues of NIFS Series

NIFS-88 N.Matsunami and K.Kitoh, *High Resolution Spectroscopy of H^+ Energy Loss in Thin Carbon Film;* May 1991

NIFS-89 H. Sugama, N. Nakajima and M.Wakatani, *Nonlinear Behavior of Multiple-Helicity Resistive Interchange Modes near Marginally Stable States;* May 1991

NIFS-90 H. Hojo and T.Hatori, *Radial Transport Induced by Rotating RF Fields and Breakdown of Intrinsic Ambipolarity in a Magnetic Mirror*; May 1991

NIFS-91 M. Tanaka, S. Murakami, H. Takamaru and T.Sato, *Macroscale Implicit, Electromagnetic Particle Simulation of Inhomogeneous and Magnetized Plasmas in Multi-Dimensions;* May 1991

NIFS-92 S. - I. Itoh, *H-mode Physics, -Experimental Observations and Model Theories-, Lecture Notes, Spring College on Plasma Physics, May 27 - June 21 1991 at International Centre for Theoretical Physics (IAEA UNESCO) Trieste, Italy ;* Jun. 1991

NIFS-93 Y. Miura, K. Itoh, S. - I. Itoh, T. Takizuka, H. Tamai, T. Matsuda, N. Suzuki, M. Mori, H. Maeda and O. Kardaun, *Geometric Dependence of the Scaling Law on the Energy Confinement Time in H-mode Discharges;* Jun. 1991

NIFS-94 H. Sanuki, K. Itoh, K. Ida and S. - I. Itoh, *On Radial Electric Field Structure in CHS Torsatron / Heliotron;* Jun. 1991

NIFS-95 K. Itoh, H. Sanuki and S. - I. Itoh, *Influence of Fast Ion Loss on Radial Electric Field in Wendelstein VII-A Stellarator;* Jun. 1991

NIFS-96 S. - I. Itoh, K. Itoh, A. Fukuyama, *ELMy-H mode as Limit Cycle and Chaotic Oscillations in Tokamak Plasmas;* Jun. 1991

NIFS-97 K. Itoh, S. - I. Itoh, H. Sanuki, A. Fukuyama, *An H-mode-Like Bifurcation in Core Plasma of Stellarators;* Jun. 1991

NIFS-98 H. Hojo, T. Watanabe, M. Inutake, M. Ichimura and S. Miyoshi, *Axial Pressure Profile Effects on Flute Interchange Stability in the Tandem Mirror GAMMA 10;* Jun. 1991

NIFS-99 A. Usadi, A. Kageyama, K. Watanabe and T. Sato, *A Global Simulation of the Magnetosphere with a Long Tail : Southward and Northward IMF;* Jun. 1991

NIFS-100 H. Hojo, T. Ogawa and M. Kono, *Fluid Description of Ponderomotive Force Compatible with the Kinetic One in a Warm Plasma* ; July 1991

NIFS-101 H. Momota, A. Ishida, Y. Kohzaki, G. H. Miley, S. Ohi, M. Ohnishi K. Yoshikawa, K. Sato, L. C. Steinhauer, Y. Tomita and M. Tuszewski *Conceptual Design of D-^{3}He FRC Reactor "ARTEMIS"* ; July 1991

NIFS-102 N. Nakajima and M. Okamoto, *Rotations of Bulk Ions and Impurities in Non-Axisymmetric Toroidal Systems* ; July 1991

NIFS-103 A. J. Lichtenberg, K. Itoh, S. - I. Itoh and A. Fukuyama, *The Role of Stochasticity in Sawtooth Oscillation* ; Aug. 1991

NIFS-104 K. Yamazaki and T. Amano, *Plasma Transport Simulation Modeling for Helical Confinement Systems;* Aug. 1991

NIFS-105 T. Sato, T. Hayashi, K. Watanabe, R. Horiuchi, M. Tanaka, N. Sawairi and K. Kusano, *Role of Compressibility on Driven Magnetic Reconnection ;* Aug. 1991

NIFS-106 Qian Wen - Jia, Duan Yun - Bo, Wang Rong - Long and H. Narumi, *Electron Impact Excitation of Positive Ions - Partial Wave Approach in Coulomb - Eikonal Approximation* ; Sep. 1991

NIFS-107 S. Murakami and T. Sato, *Macroscale Particle Simulation of Externally Driven Magnetic Reconnection;* Sep. 1991

NIFS-108 Y. Ogawa, T. Amano, N. Nakajima, Y. Ohyabu, K. Yamazaki, S. P. Hirshman, W. I. van Rij and K. C. Shaing, *Neoclassical Transport Analysis in the Banana Regime on Large Helical Device (LHD) with the DKES Code;* Sep. 1991

NIFS-109 Y. Kondoh, *Thought Analysis on Relaxation and General Principle to Find Relaxed State;* Sep. 1991

NIFS-110 H. Yamada, K. Ida, H. Iguchi, K. Hanatani, S. Morita, O. Kaneko, H. C. Howe, S. P. Hirshman, D. K. Lee, H. Arimoto, M. Hosokawa, H. Idei, S. Kubo, K. Matsuoka, K. Nishimura, S. Okamura, Y. Takeiri, Y. Takita and C. Takahashi, *Shafranov Shift in Low-Aspect-Ratio Heliotron / Torsatron CHS* ; Sep 1991

NIFS-111 R. Horiuchi, M. Uchida and T. Sato, *Simulation Study of Stepwise Relaxation in a Spheromak Plasma ;* Oct. 1991

NIFS-112 M. Sasao, Y. Okabe, A. Fujisawa, H. Iguchi, J. Fujita, H. Yamaoka and M. Wada, *Development of Negative Heavy Ion Sources for*

Plasma Potential Measurement ; Oct. 1991

NIFS-113 S. Kawata and H. Nakashima, *Tritium Content of a DT Pellet in Inertial Confinement Fusion* ; Oct. 1991

NIFS-114 M. Okamoto, N. Nakajima and H. Sugama, *Plasma Parameter Estimations for the Large Helical Device Based on the Gyro-Reduced Bohm Scaling* ; Oct. 1991

NIFS-115 Y. Okabe, *Study of Au^- Production in a Plasma-Sputter Type Negative Ion Source* ; Oct. 1991

NIFS-116 M. Sakamoto, K. N. Sato, Y. Ogawa, K. Kawahata, S. Hirokura, S. Okajima, K. Adati, Y. Hamada, S. Hidekuma, K. Ida, Y. Kawasumi, M. Kojima, K. Masai, S. Morita, H. Takahashi, Y. Taniguchi, K. Toi and T. Tsuzuki, *Fast Cooling Phenomena with Ice Pellet Injection in the JIPP T-IIU Tokamak;* Oct. 1991

NIFS-117 K. Itoh, H. Sanuki and S. -I. Itoh, *Fast Ion Loss and Radial Electric Field in Wendelstein VII-Λ Stellarator*; Oct. 1991

NIFS-118 Y. Kondoh and Y. Hosaka, *Kernel Optimum Nearly-analytical Discretization (KOND) Method Applied to Parabolic Equations <<KOND-P Scheme>>;* Nov. 1991

NIFS-119 T. Yabe and T. Ishikawa, *Two- and Three-Dimensional Simulation Code for Radiation-Hydrodynamics in ICF*; Nov. 1991

NIFS-120 S. Kawata, M. Shiromoto and T. Teramoto, *Density-Carrying Particle Method for Fluid* ; Nov. 1991

NIFS-121 T. Ishikawa, P. Y. Wang, K. Wakui and T. Yabe, *A Method for the High-speed Generation of Random Numbers with Arbitrary Distributions;* Nov. 1991

NIFS-122 K. Yamazaki, H. Kaneko, Y. Taniguchi, O. Motojima and LHD Design *Group, Status of LHD Control System Design ; Dec. 1991*

NIFS-123 Y. Kondoh, *Relaxed State of Energy in Incompressible Fluid and Incompressible MHD Fluid* ; Dec. 1991

NIFS-124 K. Ida, S. Hidekuma, M. Kojima, Y. Miura, S. Tsuji, K. Hoshino, M. Mori, N. Suzuki, T. Yamauchi and JFT-2M Group, *Edge Poloidal Rotation Profiles of H-Mode Plasmas in the JFT-2M Tokamak ;* Dec. 1991

NIFS-125 H. Sugama and M. Wakatani, *Statistical Analysis of Anomalous Transport in Resistive Interchange Turbulence* ;Dec. 1991

NIFS-126 K. Narihara, *A Steady State Tokamak Operation by Use of Magnetic Monopoles* ; Dec. 1991

NIFS-127 K. Itoh, S. -I. Itoh and A. Fukuyama, *Energy Transport in the Steady State Plasma Sustained by DC Helicity Current Drive* ;Jan. 1992

NIFS-128 Y. Hamada, Y. Kawasumi, K. Masai, H. Iguchi, A. Fujisawa, JIPP T-IIU Group and Y. Abe, *New Hight Voltage Parallel Plate Analyzer* ; Jan. 1992

NIFS-129 K. Ida and T. Kato, *Line-Emission Cross Sections for the Charge-exchange Reaction between Fully Stripped Carbon and Atomic Hydrogen in Tokamak Plasma*; Jan. 1992

NIFS-130 T. Hayashi, A. Takei and T. Sato, *Magnetic Surface Breaking in 3D MHD Equilibria of l=2 Heliotron* ; Jan. 1992

NIFS-131 K. Itoh, K. Iguchi and S. -I. Itoh, *Beta Limit of Resistive Plasma in Torsatron/Heliotron* ; Feb. 1992

NIFS-132 K. Sato and F. Miyawaki, *Formation of Presheath and Current-Free Double Layer in a Two-Electron-Temperture Plasma* ; Feb. 1992

NIFS-133 T. Maruyama and S. Kawata, *Superposed-Laser Electron Acceleration* Feb. 1992

NIFS-134 Y. Miura, F. Okano, N. Suzuki, M. Mori, K. Hoshino, H. Maeda, T. Takizuka, JFT-2M Group, S.-I. Itoh and K. Itoh, *Rapid Change of Hydrogen Neutral Energy Distribution at L/H-Transition in JFT-2M H-mode* ; Feb. 1992

NIFS-135 H. Ji, H. Toyama, A. Fujisawa, S. Shinohara and K. Miyamoto *Fluctuation and Edge Current Sustainment in a Reversed-Field-Pinch;* Feb. 1992

NIFS-136 K. Sato and F. Miyawaki, *Heat Flow of a Two-Electron-Temperature Plasma through the Sheath in the Presence of Electron Emission;* Mar. 1992

NIFS-137 T. Hayashi, U. Schwenn and E. Strumberger, *Field Line Diversion Properties of Finite ß Helias Equilibria;* Mar. 1992